Application of Three-Dimensional Digital Image Correlation to the Core-Drilling Method

Article *in* Experimental Mechanics · August 2005

DOI: 10.1007/BF02428166

CITATIONS
63

READS
203

3 authors, including:

Stephen Pessiki
Lehigh University
69 PUBLICATIONS **1,770** CITATIONS
SEE PROFILE

Hakan Tacettin Turker
Uludag University
12 PUBLICATIONS **93** CITATIONS
SEE PROFILE

Application of Three-dimensional Digital Image Correlation to the Core-drilling Method

by M.J. McGinnis, S. Pessiki and H. Turker

ABSTRACT—We present a non-destructive technique for the determination of *in situ* stresses in concrete structures, referred to as the core-drilling method. The method is similar to the American Society for Testing and Materials (ASTM) hole-drilling strain gage method, except that the core-drilling method is formulated in terms of displacement rather than strain. Measurements in the current work are performed with traditional photogrammetry, and the more novel (and more accurate) three-dimensional digital image correlation. In this paper we review the background elasticity theory and we discuss the results of verification experiments on steel plates. Calculated normal stresses are within 17% of applied values for photogrammetry, and 7% for three-dimensional digital image correlation.

KEY WORDS—Concrete, core-drilling method, hole-drilling, digital image correlation, *in situ* stress, non-destructive evaluation, photogrammetry

Nomenclature

a = hole radius
f_c' = concrete compressive strength
m = radius of measurement circle
r = distance of any point to center of hole
A, B, C, F, H, M, J = material and geometric constants
E = modulus of elasticity
U = measured displacement
$\varphi(z)$, $\kappa(z)$, $\psi(z)$, $\Phi(z)$, $\Psi(z)$ = analytic functions of complex variable
A_n, a_k, a_k' = Fourier series coefficients
σ_x, σ_y, τ_{xy} = in-plane normal and shear stresses
K_x, K_y = in-plane stress gradients
α = angle measured counterclockwise from the x-axis to the point of interest
u, v = radial and tangential relieved displacements
α_i, β, θ_{ij}, θ_{ji} = geometrical parameters (see Fig. 1)
ϕ = Airy stress function
μ = modulus of rigidity
χ = material constant for plane stress and plain strain
υ = Poisson's ratio
dx, dy, θ_z = rigid body horizontal, vertical and rotational displacements
γ_1, γ_2, γ_3 = rigid body motion scaling factors
$\Re$ = real algebraic operator

M.J. McGinnis (mjmj@lehigh.edu) is a Graduate Student and S. Pessiki is an Associate Professor, Department of Civil and Environmental Engineering, Lehigh University, Bethlehem, PA, USA. H. Turker is an Assistant Professor, Department of Civil Engineering, Mustafa Kemal University, Hatay, Turkey.

Original manuscript submitted: August 4, 2004.
Final manuscript received: April 13, 2005.
DOI: 10.1177/0014485105055435

Introduction

Reliable information about the *in situ* state of stress in the concrete in an existing structure is often needed as part of the evaluation of the structure. The evaluation may be performed as part of the determination of the load rating for the structure, or to support a decision about the repair or replacement of the structure. As just one example, information about the *in situ* state of stress in a prestressed concrete bridge girder can be used to estimate the effective prestress remaining in the girder. This information is useful in predicting the service load behavior and ultimate strength of the girder.

In this paper we present a theoretical background and the design and results of verification experiments for a non-destructive evaluation method to determine the state of stress in concrete in an existing structure. The method is referred to as the core-drilling method.[1,2] Potential applications of the method include the determination of *in situ* stress in a variety of reinforced and prestressed concrete structures, including bridges, buildings, dams, retaining walls, tunnels, shafts, and containment vessels.

In the core-drilling method, a circular core hole is cut in to the concrete in a structure, and the displacements that occur in the concrete as the hole is cut are measured. These measured displacements are then related to the *in situ* state of stress in the structure. The proposed method is non-destructive since the ability of the structure to perform its intended function is not impaired and the core hole is easily repaired. The method is similar to the American Society for Testing and Materials (ASTM) hole-drilling strain gage method (ASTM 837, 1994), which consists of measuring strains at the surface of a specimen as a hole is drilled. The ASTM hole-drilling strain gage method has been the subject of numerous technical publications, including methods to reduce the dependence of the calculations on material properties,[3] to refine the techniques involved for calculation of non-uniform stresses through depth and utilize the advantages of finite element analysis,[3–8] and to apply the technique to orthotropic materials.[9] The hole-drilling strain gage method is often used to determine residual stresses in homogenous materials such as metals. Its applicability to concrete structures is questionable because the heterogeneous nature of the concrete complicates strain measurement over small gage lengths. The current research represents a novel use of a newer class of optical displacement measurement technique, namely three-dimensional (3D) digital image correlation.[10] A random pattern of dots

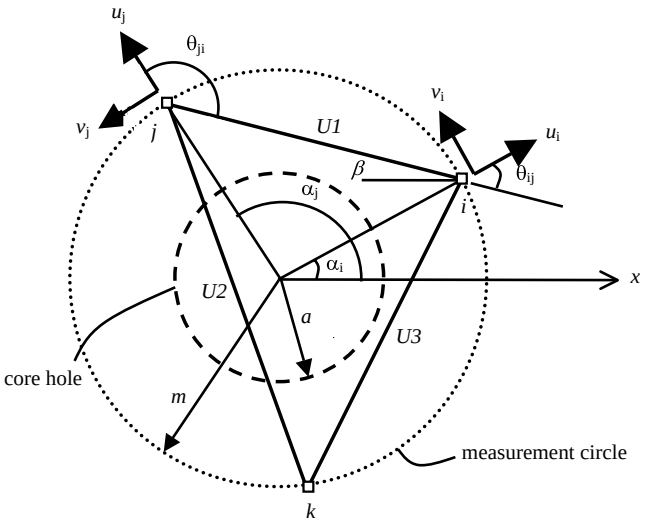

Fig. 1—Illustration of the core-drilling method showing displacement measurement between points *i* and *j*

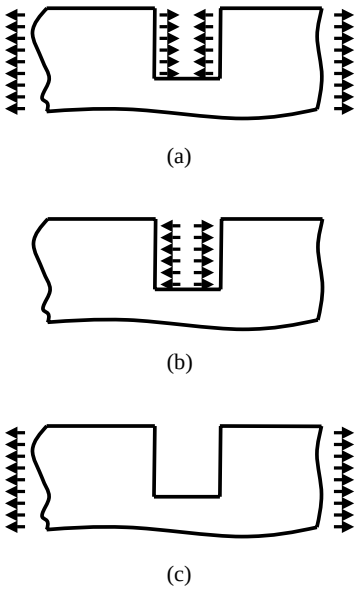

Fig. 2—Superposition of loading to find relieved displacement caused by drilling a core hole: (a) original stress; (b) relieved *in situ* stresses; (c) final stress

is photographed on the specimen, and by correlating the patterns within versions of the photographs taken before and after core drilling, deformation information is derived.

Figure 1 illustrates the proposed method. Three points, i, j, and k, are shown on the surface of the test object. As the core hole is drilled, each point undergoes a relieved displacement (u and v) relative to the center of the hole, where u and v are the radial and tangential components of the overall displacement respectively (additional information shown in Fig. 1 is discussed in the next section). Measured displacements are the relative displacement between any two of these three points, and are denoted with a capital U. These measured displacements are then related to the *in situ* stresses in the structure prior to drilling the hole. In practice, the location and number of measurement points are somewhat arbitrary. However, at least as many measurements as unknown stresses must be captured, and the measurement points should be located fairly close to the core hole to increase the magnitude of the observed displacements, and thus the accuracy of the technique. Any additional measurement points captured provide redundant data that can potentially be used to improve the accuracy of the technique.

Theory

Development of Relieved Displacement Equations

Imagine that a core hole is drilled in a structure under stress and the hole surface is subjected to equal stresses as previously existed, as shown in Fig. 2(a). The equilibrium of the body thus remains unchanged from prior to the hole drilling. In Fig. 2(b), equal and opposite stresses to those on the hole surface of Fig. 2(a) are applied at the core hole surface. The loading of Fig. 2(b) can be superposed on Fig. 2(a), resulting in the stress state after the hole is drilled (Fig. 2(c)). Thus, the loading and corresponding displacements of Fig. 2(b) are comparable to the relaxation caused by drilling the hole. In other words, the displacements caused by the loading in Fig. 2(b) are the relieved displacements.

Elasticity methods treating a small through-hole in an infinite, thin plate are used to determine the relationship between the loads and displacements of Fig. 2(b). Assumptions made in the derivations presented here are that the material is linear elastic, isotropic, homogeneous, and that the load is distributed uniformly through the plate thickness. The problem is treated as a two-dimensional problem of linear elasticity and solved for plane stress and plane strain assumptions, similar to the approach of the ASTM hole-drilling strain gage method, except that displacements rather than strains are the quantities of interest. Turker and Pessiki[1] incorporate finite elements to investigate the validity or consequences of many of these assumptions, such as the effects of blind holes, the effects of plates of finite size, and the effects of stresses that vary though the thickness of the plate.

This paper treats two related stress states in the plane of the plate, cases 1 and 2 of Fig. 3. Case 2 shows a stress state that is linearly varying in-plane, with constant shear stresses. Case 1 degenerates from case 2 if the normal stress gradients are taken to be zero. Derivations for case 1 are presented in detail herein; for case 2, a summary is presented and the interested reader is directed to Turker and Pessiki.[1]

The two-dimensional elasticity problem is solved using the potential function of complex method as outlined by Muskhelishvili.[11] The governing bi-harmonic equation for an isotropic material

$$\nabla^4\phi = \frac{\partial^4\phi}{\partial x^4} + 2\frac{\partial^4\phi}{\partial x^2\partial y^2} + \frac{\partial^4\phi}{\partial y^4} \qquad (1)$$

can be solved by finding a bi-harmonic function, $\phi(x,y)$, which satisfies the boundary conditions. If $\phi(x,y)$ is expressed in terms of analytic functions of complex variable

$$\phi(x, y) = \Re[\bar{z}\varphi(z) + \kappa(z)], \qquad (2)$$

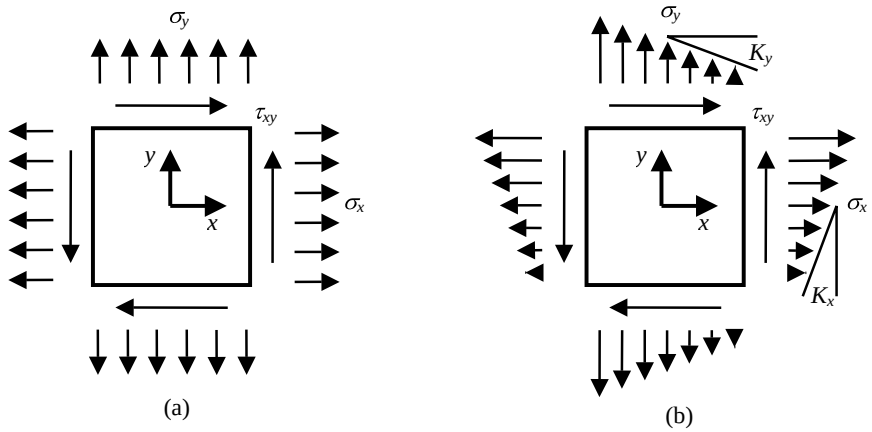

Fig. 3—Stress states treated in the core-drilling method: (a) uniform normal and shear stress; (b) biaxial linear normal stress gradient and uniform shear stress

then Muskhelishvili's normal and tangential displacement and stress equations for a polar coordinate system are given as

$$2\mu(u+\mathrm{i}v) = \mathrm{e}^{-\mathrm{i}\alpha}[\chi\varphi(z) - z\overline{\varphi'(z)} - \overline{\psi(z)}] \qquad (3)$$

$$N - \mathrm{i}T = \Phi(z) + \overline{\Phi(z)} - \mathrm{e}^{2\mathrm{i}\alpha}[\bar{z}\Phi'(z) + \Psi(z)] \qquad (4)$$

where

$$\varphi(z) = \int \Phi(z)\mathrm{d}z$$
$$\psi(z) = \int \Psi(z)\mathrm{d}z = \frac{\mathrm{d}\kappa}{\mathrm{d}z}$$

$\chi = \frac{3-\upsilon}{1+\upsilon}$ for plane stress and plane strain, respectively.
$\chi = 3 - 4\upsilon$

With static equilibrium, it can be shown that for case 1, the stresses around any circle are

$$\sigma_s = \frac{\sigma_x - \sigma_y}{2}\sin 2\alpha - \tau_{xy}\cos 2\alpha \qquad (5)$$

$$\sigma_n = \frac{\sigma_x + \sigma_y}{2} + \frac{\sigma_x - \sigma_y}{2}\cos 2\alpha + \tau_{xy}\sin 2\alpha. \qquad (6)$$

The tractions, N and T, around the core hole can also be expressed in complex Fourier expansion as

$$N - \mathrm{i}T = \sum_{-\infty}^{\infty} A_n \mathrm{e}^{-\mathrm{i}n\alpha} \qquad (7)$$

where the constants A_n are found by equating terms of like exponents with their counterparts in eqs (5) and (6), assuming that the tractions applied to the hole are the inverse of the stresses expressed in eqs (5) and (6). For case 1, the constants determined are

$$A_0 = -\frac{\sigma_x+\sigma_y}{2}$$
$$A_2 = -\frac{\sigma_x-\sigma_y}{2} + \mathrm{i}\tau_{xy} \qquad (8)$$

all other $A_n = 0$.

With complex Fourier series expansion, $\Phi(z)$ and $\Psi(z)$ for a region bounded by a circle are written as

$$\Phi(z) = \sum_{0}^{\infty} a_k z^{-k}$$
$$\Psi(z) = \sum_{0}^{\infty} a'_k z^{-k}. \qquad (9)$$

The constants a_k and a'_k are determined from the boundary conditions on the core hole circle and at infinity.

Using eq (7) to express the boundary condition on the hole (tractions are equal to the $N - \mathrm{i}T$ derived) and knowing that at infinity the stresses should be zero, the coefficients of eq (9) can be determined by equating terms with like powers of z. The coefficients thus determined are

$$a_2 = \left[-\left(\frac{\sigma_x-\sigma_y}{2}\right) - \mathrm{i}\tau_{xy}\right]a^2$$
$$a'_2 = \left(\frac{\sigma_x+\sigma_y}{2}\right)a^2 \qquad (10)$$
$$a'_4 = -3a^4\left[\left(\frac{\sigma_x-\sigma_y}{2}\right) + \mathrm{i}\tau_{xy}\right]$$

all other a_k, a'_k=0.

With $\varphi(z)$ and $\psi(z)$ now fully defined, eq (3) is applied to yield relieved displacements of

$$u = \left(\frac{\sigma_x + \sigma_y}{2}\right)A + \left(\frac{\sigma_x - \sigma_y}{2}\right)B\cos 2\alpha + \tau_{xy}B\sin 2\alpha \qquad (11)$$

$$v = \left(\frac{\sigma_x - \sigma_y}{2}\right)C\sin 2\alpha - \tau_{xy}C\cos 2\alpha \qquad (12)$$

where

$$A = \frac{a^2}{2\mu r}$$
$$B = \frac{a^2[r^2(1+\chi)-a^2)]}{2\mu r^3}$$
$$C = \frac{a^2[r^2(1-\chi)-a^2)]}{2\mu r^3}.$$

Relieved displacements give the displacement of a point relative to the center of the through-hole. However, in practice,

a displacement measurement might be taken between two points, neither of which is the center of the hole, so as to eliminate the effects of rigid body translations or rotations. Figure 1 shows a displacement measurement of this type. The measured displacement between the two measurement points, i and j, is defined in terms of relieved displacements as follows

$$U = u_i \cos\theta_{ij} - v_i \sin\theta_{ij} - u_j \cos\theta_{ji} + v_j \sin\theta_{ji} \quad (13)$$

where

$$\theta_{ij} = \alpha_i + \beta$$
$$\theta_{ji} = \alpha_j + \beta$$
$$\beta = \pi - (\alpha_i + \alpha_j)/2.$$

Determination of In Situ Stress Equations

To solve for the three unknown stresses of case 1 (σ_x, σ_y, τ_{xy}) or the five unknowns of case 2 (σ_x, σ_y, τ_{xy}, K_x, K_y), three and five measured displacements respectively are required. Either three (or five) equations expressing measured displacements in terms of *in situ* stresses must be solved simultaneously for the unknown stress quantities. In this paper, the two measurement configurations shown in Fig. 4 were used. All measurement points (shown with squares) are located on a fictitious measurement circle (shown dotted) some distance from the edge of the core hole (shown dashed). The measured displacements between two points are shown with solid lines in the figure. Using eqs (11) and (12), the measured displacements for case 1, configuration A, are as follows:

$$U1 = A(\sigma_x + \sigma_y) + B(\sigma_x - \sigma_y) \quad (14)$$

$$U2 = A(\sigma_x + \sigma_y) + 2B\tau_{xy} \quad (15)$$

$$U3 = A(\sigma_x + \sigma_y) - B(\sigma_x - \sigma_y). \quad (16)$$

Equations (14)–(16) are solved simultaneously for *in situ* stresses resulting in

$$\sigma_x = \frac{A(U1 - U3) + B(U1 + U3)}{4AB} \quad (17)$$

$$\sigma_y = \frac{A(-U1 + U3) + B(U1 + U3)}{4AB} \quad (18)$$

$$\tau_{xy} = \frac{-U1 + 2U2 - U3}{4B}. \quad (19)$$

The process outlined above (eqs (5)–(19)) for the case 1 stress state with configuration A is repeated for the case 2 stress state in conjunction with configuration B. The resulting relieved displacement and *in situ* stress equations are

$$u = \left(\frac{\sigma_x+\sigma_y}{2}\right) A + \left(\frac{\sigma_x-\sigma_y}{2}\right) B \cos 2\alpha + \tau_{xy} B \sin 2\alpha + K_x(F \sin\alpha + H \sin 3\alpha) + K_y(-F \cos\alpha + H \cos 3\alpha) \quad (20)$$

$$v = \left(\frac{\sigma_x-\sigma_y}{2}\right) C \sin 2\alpha - \tau_{xy} C \cos 2\alpha + K_x(M \cos\alpha + J \cos 3\alpha) + K_y(M \sin\alpha - J \sin 3\alpha) \quad (21)$$

$$\sigma_x = \frac{\sqrt{2}}{8AB}\left[A(U1 - U2 - U3 - U4 + 2\sqrt{2}U5) + B(-U1 + U2 + U3 + U4)\right] \quad (22)$$

$$\sigma_y = \frac{\sqrt{2}}{8AB}\left[A(-U1 + U2 + U3 + U4 - 2\sqrt{2}U5) + B(-U1 + U2 + U3 + U4)\right] \quad (23)$$

$$\tau_{xy} = \frac{\sqrt{2}}{8C}[U1 + U2 - U3 + U4] \quad (24)$$

$$K_x = \frac{\sqrt{2}}{4(F - H - M - J)}[U1 + U2 + U3 - U4] \quad (25)$$

$$K_y = \frac{\sqrt{2}}{4(F - H - M - J)}[U1 - U2 + U3 + U4] \quad (26)$$

where A, B, and C are as before (eq (13)), and

$$F = \frac{a^4}{16\mu r^2}$$
$$H = \frac{a^4}{16\mu r^4}\left[r^2(\chi + 2) - 2a^2\right]$$
$$M = -F$$
$$J = \frac{a^4}{16\mu r^4}\left[r^2(\chi - 2) + 2a^2\right].$$

Verification Experiments

Experimental Details

Two steel plates were tested in tension in these experiments, as shown schematically in Fig. 5. Plate 1 was loaded in concentric axial tension with a force P to generate a uniform stress field. Plate 2 was loaded with a similar axial load in eccentric tension at the kern point to generate a stress field that theoretically varies linearly from zero on one edge of the plate to twice the nominal value at the opposite edge.

The geometry and axial load P applied to plate 1 was designed to match the relieved displacements in a hypothetical concrete specimen with an *in situ* uniaxial compression stress of 13.8 MPa. Steel was used in the experiment instead of concrete for three reasons: (1) to provide a specimen with a known elastic modulus; (2) to provide a fine-grained, homogeneous specimen, thus eliminating any discontinuities caused by the presence of aggregates; (3) to allow the test to be performed in tension instead of compression, thereby simplifying the experiment. As noted in the discussion portion of this paper, ongoing research is involved with studying the effects of aggregate.

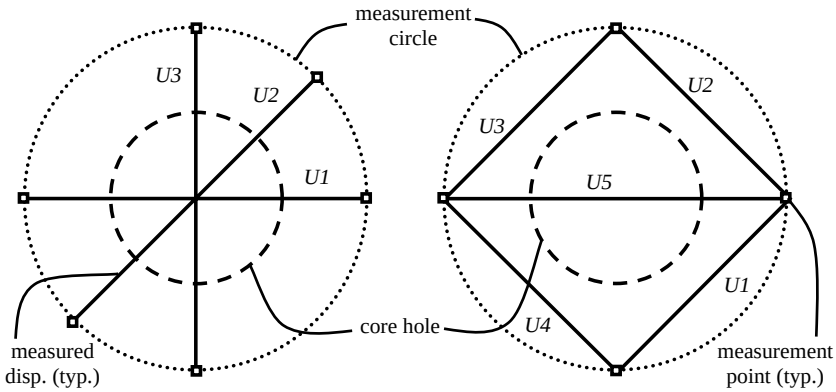

Fig. 4—Measurement configurations: (a) measurement configuration A; (b) measurement configuration B

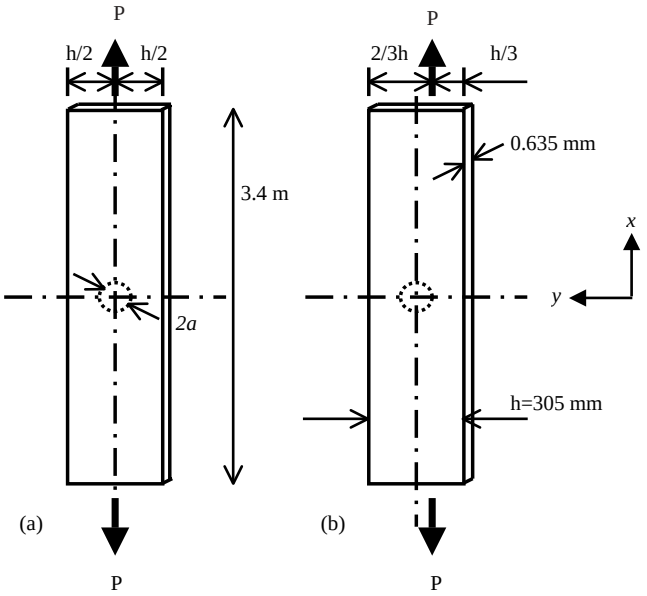

Fig. 5—Schematic diagrams of two test specimens: (a) plate 1 subjected to industrial photogrammetry; (b) plate 2 subjected to 3D digital image correlation

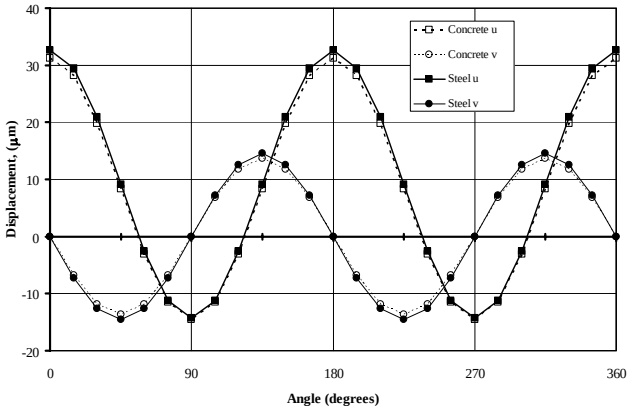

Fig. 6—Theoretical radial (u) and tangential (v) relieved displacements for the hypothetical concrete structure and representative steel plate for the uniform stress state

Table 1 shows a test matrix with the pertinent geometric, material, and load data from plate 1, plate 2, and the hypothetical concrete structure considered. Figure 6 shows the anticipated radial (u) and tangential (v) displacements for the hypothetical concrete structure and the steel test specimen used to represent the hypothetical concrete structure. The figure shows that the expected displacements of the steel test specimen closely match the hypothetical concrete specimen in both magnitude and variation around the respective measurement circles.

An arrangement of bonded wire strain gages (as visible in Fig. 7) were affixed to each side of each plate to provide verification of the expected in-plane normal stress quantities and stress gradients and to verify that there was not undue out-of-plane bending of the plate. A load cell was incorporated into the load path to measure load. Figure 7 shows the load frame used to test the two plates, with plate 1 positioned in the frame. The plates were gripped at each end by a clevis with a single load pin and loaded at one end with a hydraulic jack. The length of the plates was chosen to ensure that the load was well distributed in the center test region of each plate. The plate width was chosen so that the width to core hole diameter ratio was greater than a specified limit,[1] ensuring behavior similar to an infinite plate and thus avoiding edge effects. Further details of the experimental setup are given in McGinnis et al.[2]

Description of Measurement Techniques

Two displacement measurement techniques were evaluated and are reported here. The displacements were measured in the plate 1 test with photogrammetry. Photogrammetry is a 3D coordinate measurement technique that is widely accepted in industrial applications, although its roots are based in the field of aerial mapping. Based on triangulation principles, photogrammetry uses a series of photographs taken of the measured object from numerous angles to recreate the 3D coordinates of the targets that are placed on the object. With many different views of each target, the exact location of the target can be triangulated. This triangulation depends on knowledge of the camera's position and orientation for each photograph that is analyzed. The three major

TABLE 1—TEST MATRIX INFORMATION

Parameter	Specimen: Hypothetical Concrete Structure	Plate 1	Plate 2
Material	Concrete (f'_c = 55.2 MPa)	Steel	Steel
a	50.8 mm	28.58 mm	31.75 mm
m	76.2 mm	42.02 mm	44.45 mm
P	—	289 kN	267 kN
Eccentricity	0	0	50.8 mm
σ_x	13.8 MPa	141.2 MPa	135.5 MPa
σ_y, τ_{xy}, K_y	0	0	0
K_x	0	0	0.83 MPa/mm

Fig. 7—Load frame with plate 1 positioned for testing

analytical functions that must be performed to analyze photogrammetric data are (1) triangulation, (2) resection, and (3) self-calibration of the camera to eliminate errors such as those due to lens and camera imperfections, temperature, and humidity effects, etc. The generic term for the simultaneous mathematical calculation procedure to accomplish these three functions is "bundle adjustment".

Accuracy and precision in industrial photogrammetry are related to the size of the measured object and numerous other factors. Some factors that affect the quality of a photogrammetric survey include the resolution of the captured images, camera calibration, angles between captured photos, redundancy in the appearance of targets appearing in multiple images, and the placement of the targets. A current guideline regarding accuracy is that a quality survey (i.e., one that meets accepted standards for the influencing factors noted above, among others) can yield accuracy in coordinates of approximately one part in 80,000, with 68% probability (1 sigma). Thus, as an example, for a measured object size of 1 m, one would expect accuracy in coordinates to 13 μm. However, typical surveys are of areas often larger than several square meters. With all other factors equal, the strong dependence on scale means that industrial photogrammetry applied with a measured object size substantially smaller than 1 m can greatly reduce this uncertainty in measured coordinates.

For this study, a non-metric black and white digital camera with a six megapixel charge-coupled device (CCD) was used to capture a series of approximately 30 photographs of the specimen from many different angles at a distance of 1–2 m. The camera was equipped with a 24 mm manual focus lens. Custom non-reflective targets were used for this exercise, and as part of the photogrammetry bundle-adjustment protocol, the camera was self-calibrated on-site.

The displacements were measured in the plate 2 test with 3D digital image correlation. 3D digital image correlation[10] combines techniques of image correlation with the photogrammetric location principles described above, and is practical only with the advent of high-speed computers. Sample preparation consists of applying a regular or random pattern with good contrast to the surface of the measured object. The pattern will then deform with the object under load. The object is captured in a stereo pair of high-quality cameras while it is loaded. These two cameras are mounted at either end of a base bar such that their relative position and orientation with respect to one another is fixed and known. In this case, many of the photogrammetric principles noted above reduce to mathematically simpler forms than for classical photogrammetry. The optimum total angle between the two cameras is 25°. Lower angles will reduce the accuracy of the triangulation, and thus reduce the accuracy of the out-of-plane (z-axis) coordinates and displacements. Wider angles increase the accuracy of the z coordinates, but the increased perspective reduces the useful field of view.

Thousands of unique correlation areas known as facets (typically 15 square pixels for the system used herein) are defined across the entire imaging area. The center of each facet is a measurement point that is tracked, in each successive pair of images, with accuracy up to one hundredth of a pixel by employing a similarity measure such as the normalized cross-correlation. An image correlation algorithm, as for example, the iterative spatial domain cross-correlation algorithm, tracks facets by maximizing this similarity measure. The 3D locations of these facets are calculated before and after each load step, yielding displacements. Tracking the dense cloud of points within the applied pattern provides displacement information that is "near" full-field.

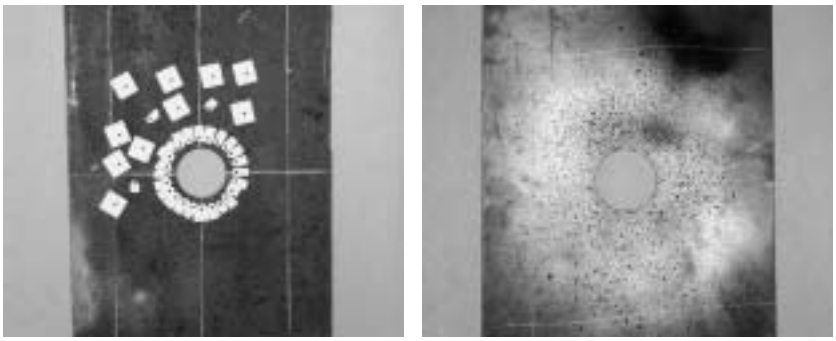

(a) (b)

Fig. 8—Photographs of plates after coring: (a) plate 1 subjected to photogrammetry; (b) plate 2 subjected to 3D digital image correlation

3D image correlation is often more practical than other full-field methods that require interferometric stability between the sensor and test part in order to acquire data. In 3D image correlation, significant rigid body motions can first be quantified and then removed. Since strains are calculated from the derivative of displacement, rigid body motion is intrinsically eliminated from strain data in 3D image correlation photogrammetry. As long as non-blurred pictures can be captured, 3D coordinates, displacements, and strains can be measured. Although not utilized herein, this means that the technology can be tailored to situations involving measurement in the dynamic environment.

The 3D image correlation system is calibrated using National Institute of Standards and Technology traceable calibration panels for each field of view. A sequence of pictures of the panel at different distances and orientations is captured and a bundle adjustment used to establish the precise relationship between the two cameras. Each dot on the calibration panel occupies more than 100 pixels on each camera sensor, so dot centers can be interpolated to an accuracy of at least 1/30 of a pixel. The resolution of the technique necessarily follows many of the same prescripts noted above for industrial photogrammetry, as well as being influenced by the accuracy of the image correlation algorithm. Since there are 1280 $\times$ 1024 pixels on the Vosskuhler CCD-1300 digital cameras used for these tests, the overall accuracy of the system used herein can be conservatively stated as 1/30,000 the field of view. For a 10 mm field of view, for example, this equates to 0.33 μm displacement sensitivity. The displacement sensitivity scales linearly with the field of view, decreasing to 3 μm at for a field of view of 100 mm and 30 μm at 1 m, assuming 1280 pixels across the field of view. In the current work, after calibration of the system on-site, the image pairs were captured at a distance near 1 m from the specimen, with a field of view of approximately 150 mm.

Experimental Results

Figure 8 shows photographs of the two plates after coring. Figure 8(a) is plate 1 subjected to traditional photogrammetry, and Fig. 8(b) is plate 2 subjected to 3D digital image correlation. Shown in these photographs are the manually placed discrete targets used in the traditional photogrammetry, and the "spluttered" spray paint applied for the 3D digital image correlation. Each plate was loaded as described above. A reading was taken with the given displacement measurement technique, and then a core hole was cut in the plate. After coring, a second reading was taken to determine the relieved displacements.

Figure 9 compares the measured displacements with the theoretical displacements from both plates. In the figure, rigid body motions have been removed from each measured displacement quantity. This was accomplished by the subtraction from the displacement output for each technique of terms such as $\gamma_1 \mathrm{d}x$, $\gamma_2 \mathrm{d}y$, and $\gamma_3 \theta_z$, scaled displacements in the horizontal, vertical, and rotational directions respectively. γ_1, γ_2, and γ_3 were varied to minimize the root sum square difference between the measured and theoretical relieved displacements. Note that the subtraction from the relieved displacements of rigid body translations and a rigid body rotation has no impact on the stress solutions, as eqs (17)–(19) and (22)–(26) are expressed in terms of measured displacements, i.e., as the difference between two relieved displacements. For plate 1, the measurement radius considered was 42 mm, for plate 2, 44 mm. 3D digital image correlation provided displacement values for thousands of discrete points on the surface of the plate; only a few are shown here. Further consideration of the richness of this data set beyond that considered here would almost certainly improve the accuracy of the stress measurements presented in the following section. In general, good agreement is obtained between the measured and theoretical displacements. This suggests that the two measurement techniques provide acceptable accuracy for the problem of interest (stresses in concrete).

Equations (17)–(19) and (22)–(26) were applied to plates 1 and 2 respectively to determine the *in situ* stress in each plate. Table 2 shows the measured stress quantities for each plate tested as well as the relative errors in each quantity versus the applied value. In each case, the measured values are the results of averaging the stress quantities obtained from configuration A or B every 15° around the measurement circle.

Discussion

For the plate 1 test, the calculated stress results are within 17% of the applied stress quantities—encouraging for a first test of the technique. In an actual field test on a concrete structure, the modulus of elasticity, E, of the concrete would

TABLE 2—EXPERIMENTAL RESULTS FOR PLATE 1 AND PLATE 2

Specimen	Measured Quantity	Stress Results: Magnitude (MPa or MPa/mm)	Stress Results: Percentage Difference from Applied σ_x or K_x
Plate 1 photogrammetry	σ_x	117.4	–16.9
	σ_y	4.6	3.3
	τ_{xy}	6.5	4.6
Plate 2 3D digital image correlation	σ_x	126.3	–6.8
	σ_y	6.9	5.1
	τ_{xy}	1.2	–0.9
	K_x	0.56	–32.5

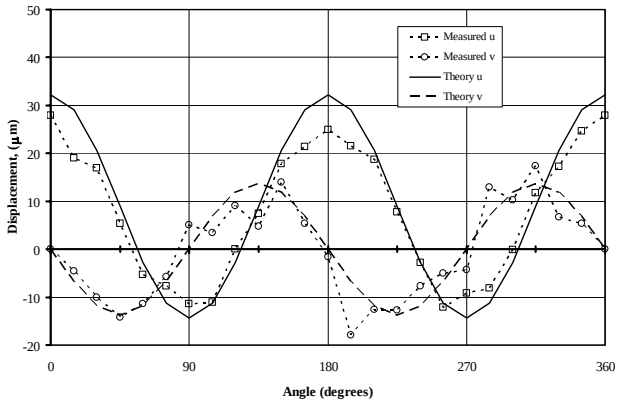

(a)

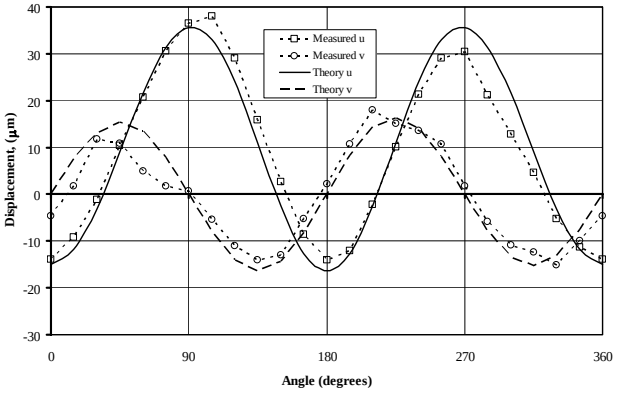

(b)

Fig. 9—Theoretical and measured radial (u) and tangential (v) displacements from: (a) plate 1; (b) plate 2

be determined from the core taken and would likely be determined within 10–15%; so these results are certainly within this uncertainty range. Further, as this was the first use of traditional photogrammetry for this application, the targets were placed manually, resulting in a certain amount of relative positional error that was not accounted for in the equations as currently conceived. A simple, prefabricated target array that could be affixed to the specimen would likely improve the accuracy of the technique.

Excellent results (less than 7% error in normal stress) were obtained with 3D digital image correlation. The reason for the relatively high error in the calculation for K_x is unknown at this time and warrants further study. One possibility is that the relative magnitude of the relieved displacements due to the bending (linear gradient) portion of the applied stress field is significantly smaller than that for the normal (constant) portion of the applied stress field, and thus the linear gradient terms are more difficult to capture experimentally. As stated previously, 3D digital image correlation captures thousands of points; however, here only a relative scarcity (<30) points were used to perform the *in situ* stress calculations. It is likely that a numerical scheme involving a much larger subset of the available data would increase the accuracy in the K_x predictions.

It has been shown in the current paper that photogrammetry and 3D digital image correlation are robust enough to capture the expected displacements involved in a typical concrete structure subjected to the core-drilling method. This conclusion is drawn based on measurements performed on specimens made of steel, a fine-grained homogeneous material. Ongoing work investigates some of the further complications of the technique as applied to concrete, among them:

- allowance for moisture induced deflections (e.g., swelling from moisture uptake during the wet coring process);
- allowance for changes in expected stress distributions due to creep, shrinkage and the presence of steel reinforcement; and
- the influence of coarse aggregate size, gradation, and volume fraction.

Acknowledgments

This research was funded by the Pennsylvania Infrastructure Technology Alliance. Additional support was provided by the Precast/Prestressed Concrete Institute, the Center for Advanced Technology for Large Structural Systems, and by Lehigh University. Additional support for the image correlation and photogrammetry measurements was provided by Trilion Quality Systems, Pennsylvania, and by Accurex Dimensional Measurement, New Jersey. The support noted above is gratefully acknowledged.

References

1. Turker, H. and Pessiki, S., "Theoretical Development of the Core-drilling Method for Non-destructive Evaluation of Stresses in Concrete

Structures," Report No. 03-07, Center for Advanced Technology for Large Structural Systems, Lehigh University, 249 pp (2003).

2. McGinnis, M.J., Pessiki, S., and Turker, H., "Application of 3D Image Correlation Photogrammetry and Classical Photogrammetry to the Core-drilling Method for Measuring In Situ Stresses in Concrete Structures," Report No. 04-16, Center for Advanced Technology for Large Structural Systems, Lehigh University, 50 pp (2004).

3. Schajer, G.S., "Application of Finite Element Calculations to Residual Stress Measurements," Journal of Engineering Materials and Technology, **103** *(2), 157–163 (1981).*

4. Schajer, G.S., "Measurement of Non-uniform Residual Stresses Using the Hole-drilling Method. Part I," Transactions of ASME, **110** *(4), 338–343 (1988).*

5. Schajer, G.S., "Measurement of Non-uniform Residual Stresses Using the Hole-drilling Method. Part II," Transactions of ASME, **110** *(4), 344–349 (1988).*

6. Beghini, M., "Recent Advances in the Hole Drilling Method for Residual Stress Measurement," Journal of Materials Engineering and Performance, **7** *(2), 163–172 (1998).*

7. Beghini, M., "Analytical Expression of the Influence Functions for Accuracy and Versatility Improvement in the Hole-drilling Method," Journal of Strain Analysis, **35** *(2), 125–135 (2000).*

8. Flaman, M.T., "Determination of Residual Stress Variation with Depth by the Hole-drilling Method," EXPERIMENTAL MECHANICS, **25** *(9), 205–207 (1985).*

9. Schajer, G.S. and Yang, L., "Residual Stress Measurement in Orthotropic Materials Using the Hole-drilling Method," EXPERIMENTAL MECHANICS, **34** *(4), 324–333 (1994).*

10. Tyson, J., Schmidt, T., and Galanulis, K., "Advanced Photogrammetry for Robust Deformation and Strain Measurement," Proceedings of SEM 2002 Annual Conference, Milwaukee, WI, June (2002).

11. Muskhelishvili, N.I., Some Basic Problems of the Mathematical Theory of Elasticity, 4th corrected and augmented edition, J.R.M. Radok (translator), P. Noordhoff, Groningen, the Netherlands (1954).